Exploring high transition temperature topological superconductivity in (Li$_{1-x}$Co$_x$OH)CoSb superlattices

M. U. Muzaffar [●],[1] Wenjun Ding [●],[1] Shunhong Zhang [●],[1] Ping Cui [●],[1,2,*] and Zhenyu Zhang [●][1,†]

[1]*International Center for Quantum Design of Functional Materials (ICQD), Hefei National Laboratory for Physical Sciences at Microscale (HFNL), and CAS Center for Excellence in Quantum Information and Quantum Physics, University of Science and Technology of China, Hefei, Anhui 230026, China*

[2]*Key Laboratory of Strongly-Coupled Quantum Matter Physics, Chinese Academy of Sciences, School of Physical Sciences, University of Science and Technology of China, Hefei, Anhui 230026, China*

Among the FeSe-based superconductors, (Li$_{1-x}$Fe$_x$OH)FeSe has been discovered as an air-stable superlattice structure harboring both high transition temperature (high-T_c) superconductivity and intriguing topological superconducting properties. Here, we use first-principles approaches to identify a chemically isovalent and structurally identical counterpart of (Li$_{1-x}$Fe$_x$OH)FeSe, namely, (Li$_{1-x}$Co$_x$OH)CoSb, which not only is an attractive candidate to harbor high-T_c superconductivity, but also exhibits two distinct features surrounding topology and magnetism. The rationale of this predictive design is based on the recent identification of CoSb as a layered high-T_c superconductor stabilized on SrTiO$_3$. We first show that the superlattice structures of (Li$_{1-x}$Co$_x$OH)CoSb ($x = 0$ or 0.25) are dynamically and thermodynamically stable. Next, we demonstrate that (Li$_{1-x}$Co$_x$OH)CoSb possesses superior superconducting properties to (Li$_{1-x}$Fe$_x$OH)FeSe, offering an appealing platform for realizing high-T_c superconductivity beyond the Cu- and Fe-based superconducting systems. More strikingly, we find that (LiOH)CoSb is already topologically nontrivial even without extrinsic doping in the spacer layers, thereby offering a cleaner and more ideal candidate system for realizing topological superconductivity. Furthermore, (Li$_{1-x}$Co$_x$OH)CoSb exhibits weaker elemental magnetic moments than (Li$_{1-x}$Fe$_x$OH)FeSe, which may provide a different angle for elucidating the microscopic mechanisms of superconductivity in these and related systems.

DOI: 10.1103/PhysRevB.102.174513

I. INTRODUCTION

Over the last decade, FeSe has been a focus of research in exploration of high transition temperature (high-T_c) superconductivity [1–3] and topological superconductivity [4–6]. The relatively simple crystalline structure and two-dimensional (2D) nature of FeSe render versatile tunability on its superconducting characteristics [7]. For example, by placing one-unit-cell FeSe films on proper oxide substrates [8–10], or by intercalating bulk FeSe with alkali atoms [11], small molecules [12], or spacer layers [13,14], substantially enhanced T_c can be achieved. In particular, (Li$_{1-x}$Fe$_x$OH)FeSe has been discovered as an air-stable superlattice structure harboring high T_c's (over 42 K) [13,14], improved single crystalline phases [13], and heavily electron-doped band structures [15,16]. More recently, identification of topological superconductivity has also been observed in FeTe$_{0.55}$Se$_{0.45}$ [4,5] and (Li$_{0.84}$Fe$_{0.16}$OH)FeSe [6]. In these systems, the topological nature of the electronic structure and s-wave superconductivity may coexist and integrate to form a different type of topological superconductor in bulk form [17–19], in contrast to the heterostructure-based topological superconductors rooted in proximity effects [20–22]. These experimental advances have stimulated significant

efforts on revealing the underlying superconducting mechanisms [3,23–29] and providing stronger evidence for the existence of topological superconductivity [30–33]. Such improved understandings may also lead to the discovery of new superconductors with potentially even higher T_c and technologically more significant topological properties.

Indeed, extensive efforts have been made along the above line. As a compelling example, in a comprehensive research project on seeking new superconductors and functional materials, tens of superconductors had been found out of $\sim$1000 materials investigated [34]. However, none of these superconductors have been shown to exhibit high-T_c superconductivity beyond the Cu- and Fe-based superconductor families. In those earlier studies, attention was mainly focused on materials with layered bulk structures [34]. On the other hand, more recent studies revealed that materials that do not prefer layered bulk structures may also be stabilized as monolayers in the two-dimensional (2D) limit [35,36]. In particular, a 2D superconducting building block, namely, monolayered CoSb, has been predicted, which possesses an identical crystal structure and the same number of valence electrons as FeSe [37]. Motivated by this prediction, monolayered CoSb films with different symmetries have been successfully synthesized on SrTiO$_3$ (STO) substrates and observed to exhibit high-T_c superconducting-like gaps by scanning tunneling spectroscopy (STS) [38,39]. More recently, a CoSb-intercalated system of LaCoSb$_2$ has also

been proposed to host possible *p*-wave superconductivity in its doped form [40]. These latest developments have effectively broadened our candidate material space as we search for new superconductors that might simultaneously exhibit high-T_c superconductivity and nontrivial topology.

In this paper, we use first-principles approaches to identify a chemically isovalent and structurally identical counterpart of $(Li_{1-x}Fe_xOH)FeSe$, namely, $(Li_{1-x}Co_xOH)CoSb$, which not only is an attractive candidate to harbor high-T_c superconductivity as well, but also exhibits two distinct features surrounding topology and magnetism. We first show that the superlattice structures of $(Li_{1-x}Co_xOH)CoSb$ ($x = 0$ or 0.25) constructed by stacking the CoSb superconducting monolayers and $(Li_{1-x}Co_xOH)$ spacer layers vertically are both dynamically and thermodynamically stable. Next, we demonstrate that $(Li_{1-x}Co_xOH)CoSb$ possesses superconducting properties comparable with or superior to $(Li_{1-x}Fe_xOH)FeSe$, which can be mainly attributed to the isovalent nature between these two systems. More strikingly, we find that (LiOH)CoSb is already topologically nontrivial even without any extrinsic doping in the spacer layers, in sharp contrast to its counterpart of $(Li_{1-x}Fe_xOH)FeSe$, which is trivial in the undoped case [6]. Therefore, (LiOH)CoSb should offer an intrinsically cleaner and more ideal candidate system for realizing topological superconductivity. Furthermore, $(Li_{1-x}Co_xOH)CoSb$ exhibits distinctly different magnetic properties from $(Li_{1-x}Fe_xOH)FeSe$, which may provide a different angle for elucidating the dominant microscopic mechanisms of high-T_c superconductivity in these and related systems.

II. METHODS

The energetic calculations and structural relaxations were performed within density functional theory (DFT) by using the Vienna *ab initio* simulation package (VASP) [41]. Valence electrons were described using the projector-augmented wave (PAW) method [42]. The exchange and correlation functional was treated using the Perdew-Burke-Ernzerhof (PBE) parametrization of generalized gradient approximation (GGA) [43]. The kinetic-energy cutoff of the plane-wave basis was chosen to be 400 eV for both the $(Li_{1-x}Co_xOH)CoSb$ and $(Li_{1-x}Fe_xOH)FeSe$ systems. A Γ-centered $15\times15\times9$ Monkhorst-Pack *k*-mesh was used for Brillouin-zone sampling. Electronic minimizations were performed with an energy tolerance of 10^{-6} eV, and optimized atomic structures were achieved when the forces on all the atoms were smaller than 0.01 eV/Å. For the layered superlattice structures, the van der Waals (vdW) interaction was included via the vdW-DF2 method [44], and the cohesive energy was defined as $E_c = E_{SC} + E_{SP} - E_{Bulk}$, where E_{SC}, E_{SP}, and E_{Bulk} represent the total energies of the superconducting layers (CoSb or FeSe), spacer layers $(Li_{1-x}Co_xOH$ or $Li_{1-x}Fe_xOH)$, and combined bulk structures $[(Li_{1-x}Co_xOH)CoSb$ or $(Li_{1-x}Fe_xOH)FeSe]$, respectively. The charge density difference was defined as $\Delta\rho_z = \rho_{Bulk} - \rho_{SC} - \rho_{SP}$, where ρ_{Bulk}, ρ_{SC}, and ρ_{SP} represent the plane-averaged charge densities along the *c* axis of the combined bulk superlattice structures, superconducting layers, and spacer layers, respectively. The spin-orbit coupling

(SOC) effects were considered in all the band-structure calculations. To investigate the magnetic properties and electron-electron correlation effects in both $(Li_{1-x}Co_xOH)CoSb$ and $(Li_{1-x}Fe_xOH)FeSe$, the on-site Coulomb interaction (Hubbard *U* correction) was added on the *d* electrons of the Co or Fe atoms using the default setting in VASP (LDAUTYPE = 2) [45]. To investigate the potential existence of the topological surface states (TSSs), the surface Green's functions of semi-infinite slabs were calculated from maximally localized Wannier functions [46] by using the WannierTools package [47]. Such Wannier functions also allow an independent determination of the topological invariants. The band characters were analyzed by using the method of elementary band representations (EBRs) [48,49] as implemented in the vasp2trace code [50], which is widely used to identify nontrivial topology [51–53].

Phonon dispersions were obtained by using the density functional perturbation theory (DFPT) as coded in the QUANTUM-ESPRESSO package [54]. Troullier-Martins norm-conserving scheme [55] was used to generate pseudopotentials for both $(Li_{1-x}Co_xOH)CoSb$ and $(Li_{1-x}Fe_xOH)FeSe$ systems. The kinetic-energy cutoff was chosen to be 70 Ry for both $(Li_{1-x}Co_xOH)CoSb$ and $(Li_{1-x}Fe_xOH)FeSe$. The dynamical matrices and electron-phonon coupling (EPC) matrices were computed with *k*-meshes of $18\times18\times18$, $12\times12\times8$ and *q*-meshes of $3\times3\times3$, $2\times2\times2$ for the corresponding systems at $x = 0$ and 0.25, respectively. The EPC strength was calculated from the isotropic version of the Eliashberg function $\alpha^2F(\omega)$ as [[56–58]:

$$\lambda = 2 \int_0^\infty \frac{\alpha^2F(\omega)}{\omega} d\omega, \tag{1}$$

where ω is the phonon frequency. The T_c was calculated using the McMillan-Allen-Dynes parametrized Eliashberg equation [56–58]:

$$k_B T_c = \frac{\hbar\omega_{log}}{1.2} \exp\left[-\frac{1.04(1+\lambda)}{\lambda - \mu^*(1+0.62\lambda)}\right], \tag{2}$$

$$\omega_{log} = \exp\left[\frac{2}{\lambda} \int_0^\infty d\omega \frac{\alpha^2F(\omega)}{\omega} ln\omega\right], \tag{3}$$

where ω_{log} is the logarithmically averaged phonon frequency, and μ^* is a parameter describing the Coulomb repulsion which usually takes values in the range of 0.1–0.2 [58]. Here we used $\mu^* = 0.1$ in our estimations.

The *ab initio* molecular dynamics (AIMD) simulations were performed as implemented in VASP to verify the thermodynamic stability of $(Li_{1-x}Co_xOH)CoSb$. The canonical *NVT* (*N*: number of particles; *V*: volume; *T*: temperature) ensemble was adopted with a Nosé thermostat [59]. The supercells of $\sqrt{2}\times\sqrt{2}\times1$, $2\sqrt{2}\times2\sqrt{2}\times1$ and *k*-meshes of $7\times7\times7$, $5\times5\times5$ were used for $(Li_{1-x}Co_xOH)CoSb$ at $x = 0$ and 0.25, respectively. The time step was set to 2 fs and the AIMD simulations were conducted for more than 4000 steps (8 ps) at 100 K.

III. RESULTS

In this work, a superlattice structure, namely $(Li_{1-x}Co_xOH)CoSb$ ($x = 0$ or 0.25), has been constructed by stacking the CoSb monolayers and the $(Li_{1-x}Co_xOH)$
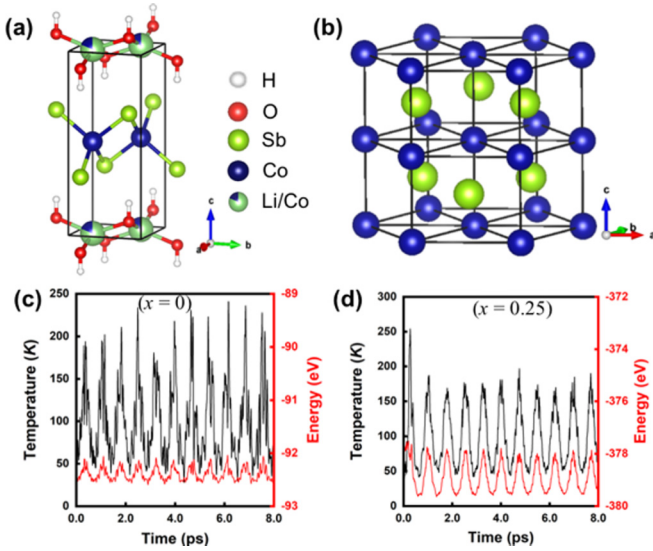
FIG. 1. (a) Tetragonal crystalline structures of $(Li_{1-x}Co_xOH)CoSb$ ($x = 0$ and 0.25), in which the superconducting layer CoSb has a layered structure identical to FeSe. (b) Crystal structure of NiAs-type CoSb. (c), (d) AIMD simulation results for $x = 0$ and 0.25, respectively.

layers vertically together along the c axis [Fig. 1(a)]. Here the monolayered CoSb is used as the essential building block for constructing the high-T_c superconductors [37]. Due to the stronger SOC effects of the heavier element (Sb), it may also offer opportunities by combining nontrivial topology with superconductivity [60]. Here, it is natural to choose $(Li_{1-x}Co_xOH)$ as the spacer layers of the superlattice structure. We use $x = 25\%$ of Co doping in the $(Li_{1-x}Co_xOH)$ spacer layers as a representative case for inducing electron doping effects, close to that of the high-T_c $(Li_{1-x}Fe_xOH)FeSe$ systems [13,14]. While bulk FeSe prefers the tetragonal PbO-type layered structure, making it easier to be stabilized as a free-standing or supported FeSe monolayer, bulk CoSb prefers the NiAs-type structure with no resemblance to layering [61,62], as shown in Fig. 1(b). Nevertheless, given the isovalency nature of the two systems, we still expect that CoSb can be stabilized in the superlattice structure of $(Li_{1-x}Co_xOH)CoSb$ just like $(Li_{1-x}Fe_xOH)FeSe$, as confirmed in the calculated results below.

The section is organized as follows: We first examine the energetics and stabilities of (LiOH)CoSb in Sec. III A; we then investigate the electronic structures and superconducting properties of (LiOH)CoSb in Sec. III B; we further explore the enhanced stability, interlayer charge transfer, and superconductivity of $(Li_{1-x}Co_xOH)CoSb$ in Sec. III C; next, we demonstrate the nontrivial topology of (LiOH)CoSb in Sec. III D; and finally, we present the magnetic properties of $(Li_{1-x}Co_xOH)CoSb$ in Sec. III E.

A. Energetics and stabilities of (LiOH)CoSb

We first examine the energetic, dynamic, and thermodynamic stabilities of the undoped (LiOH)CoSb system

TABLE I. Calculated structural parameters (a, c) and cohesive energy E_c for both the $(Li_{1-x}Co_xOH)CoSb$ and $(Li_{1-x}Fe_xOH)FeSe$ superlattice systems in the non-spin-polarized scheme with SOC. For comparison, the optimized lattice constants obtained without SOC are presented in the parentheses as references.

	$(Li_{1-x}Co_xOH)CoSb$		$(Li_{1-x}Fe_xOH)FeSe$	
	$x = 0$	$x = 0.25$	$x = 0$	$x = 0.25$
a (Å)	3.84 (3.77)	3.95	3.76 (3.71)	3.83
c (Å)	11.13 (10.70)	10.07	10.10 (10.02)	9.05
E_c (eV/f.u.)	0.16	0.28	0.17	0.32

via structural optimization, phonon dispersion analysis, and AIMD simulations. As shown in Table I, (LiOH)CoSb possesses optimized lattice constants of $a = 3.84$ Å and $c = 11.13$ Å with SOC effects included. The lattice constants of (LiOH)CoSb have been increased $\sim 4\%$ vertically and $\sim 2\%$ laterally by the inclusion of the SOC effects, while the lattice constants of (LiOH)FeSe remain almost intact (changed by less than 1%) with or without considering SOC. These major differences can be attributed to the much stronger SOC effects of Sb than that of Se (i.e., the SOC constant for a neutral Sb atom is 0.40 eV, while for a neutral Se atom is 0.22 eV) [63]. We find that the SOC effects are much stronger in (LiOH)CoSb than (LiOH)FeSe, a subtle point relevant to the discussions of their topological properties later. (LiOH)CoSb also possesses a slightly larger cell volume than that of (LiOH)FeSe due to the larger atomic radius of Sb, as well as different bond distances and bond angles, as shown in Table II. Furthermore, the cohesive energy of (LiOH)CoSb is 0.16 eV/formula unit (f.u.) and the average bond distance of the nearest H-Sb is 3.5 Å, indicating that the interlayer couplings between the CoSb layers and the (LiOH) spacer layers are of the weak vdW type. As shown in Fig. 3(a), the calculated phonon spectrum of (LiOH)CoSb exhibits no imaginary frequency, indicating that the system is dynamically stable. Moreover, our AIMD simulations at 100 K and up to 8 ps demonstrate that the system is thermodynamically stable as well, as presented in Fig. 1(c).

TABLE II. Interatomic distances and interatomic angles for both the (LiOH)CoSb and (LiOH)FeSe systems after full relaxation with SOC. The top or bottom Sb atoms refer to that in the top or bottom layer of a CoSb monolayer in triatomic-layer geometry, respectively.

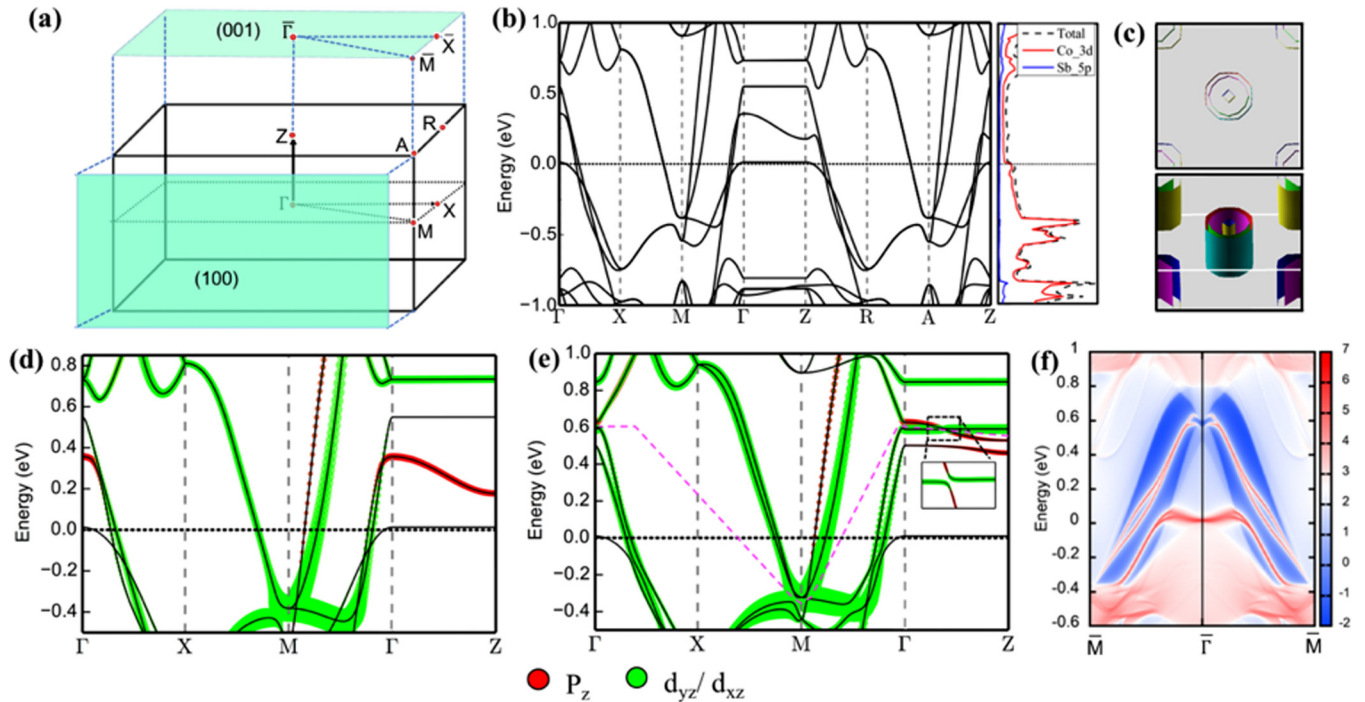| Interatomic distances (Å)			
Co-Sb	2.6	Fe-Se	2.4
H-Sb	3.5	H-Se	2.3
O-H	1.0	O-H	1.0
Interatomic angles (degree)			
$Sb^{(top)}$-Co-$Sb^{(top)}$	98	$Se^{(top)}$-Fe-$Se^{(top)}$	106
$Sb^{(top)}$-Co-$Sb^{(bottom)}$	116	$Se^{(top)}$-Fe-$Se^{(bottom)}$	111
O-H-Sb	128	O-H-Se	125

FIG. 2. (a) The first Brillouin zone (BZ) and the projected (001) and (100) surfaces of (LiOH)CoSb with the high-symmetry points indicated. (b) The electronic band structure, the projected density of states (DOS), and (c) the Fermi surfaces of (LiOH)CoSb without SOC. The projected band structures of (LiOH)CoSb without and with SOC are presented in (d) and (e), respectively. Here, the sizes of the red and green circles denote the spectral weights contributed by the p_z and d_{yz}/d_{xz} orbitals of Sb and Co ions, respectively. Note that the two flat bands with the band characters $d_{x^2-y^2}$ and d_{xy} along Γ-Z path are not contributing to the band inversion, so their projections are not displayed here. The magenta dashed line in (e) corresponds to a Fermi curve across the gap, while the inset shows a zoomed-in view of the selected area. (f) Band structure projected onto the (100) surface of the corresponding system. The Fermi level is set at 0 eV in all band structure and DOS plots.

B. Electronic structures and superconducting properties of (LiOH)CoSb

Next we turn our attention to the electronic structures and superconducting properties of the undoped system of (LiOH)CoSb. As shown in Fig. 2(b), the band structure of (LiOH)CoSb exhibits metallic features, with five bands across the Fermi level. An analysis of the partial density of states (PDOS) shows that these electronic states around the Fermi level are mainly contributed by the $3d$ electrons of Co. As shown in Fig. 2(c), the Fermi surfaces of (LiOH)CoSb contain five cylinder-like Fermi surface sheets, corresponding to the three-hole pockets and two-electron pockets in the band structures around the Γ point and the M point, respectively. These features in the electronic structures of (LiOH)CoSb are in close similarity with that of (LiOH)FeSe [64], which can be mainly attributed to the isovalent nature of the two systems and may also lead to comparable superconducting properties.

We then examine the superconducting properties of (LiOH)CoSb. To date, the dominant pairing mechanisms in the FeSe-based superconductors have been actively debated, with antiferromagnetic/orbital fluctuations [23,24,65–68], EPC [3,25–29], or the resultant effect of these [3,25,68] to be frequently invoked. Here we use the EPC strength as a quantitative indicator for superconductivity, especially because more recent studies have strongly supported its importance in enhancing the T_c's of the FeSe-based superconductors [3,25–29]. Figures 3(a) and 3(b) display the calculated

phonon linewidth, isotropic Eliashberg function $\alpha^2 F(\omega)$, and EPC strength λ of (LiOH)CoSb in comparison with that of (LiOH)FeSe. The calculated results show that the EPC strength λ is 0.43 for (LiOH)CoSb, $\sim$1.5 times larger than that of (LiOH)FeSe ($\lambda = 0.31$). By using the McMillan-Allens-Dynes parametrized Eliashberg equation [see Eq. (2) in the Methods section] with the empirical Coulomb repulsion parameter $\mu^* = 0.1$, the T_c of (LiOH)CoSb is estimated to be 0.62 K, also higher than that of (LiOH)FeSe ($T_c \sim 0.14$ K). Qualitatively, the higher T_c for the (LiOH)CoSb can be attributed to the phonon softening effects shown in Fig. 3(c), which may lead to a compensation effect on T_c [see Eqs. (2) and (3) in the Methods section]. Even though the EPC strength λ and T_c of FeSe and related systems can be substantially underestimated by the DFT-based linear response calculations [27,69–71], the present results do indicate that (LiOH)CoSb possesses superconducting properties comparable with or even superior to that of (LiOH)FeSe based on the EPC scheme. It should be reminded that the estimated T_c is only an indicator, and is expected to be substantially enhanced upon carrier doping, as well as upon proper inclusion of the strong electron correlations [72].

C. Enhanced stability, interlayer charge transfer, and superconductivity in (Li$_{0.75}$Co$_{0.25}$OH)CoSb

The next, and more crucial, issue is to investigate the doped superlattice structures of (Li$_{1-x}$Co$_x$OH)CoSb,
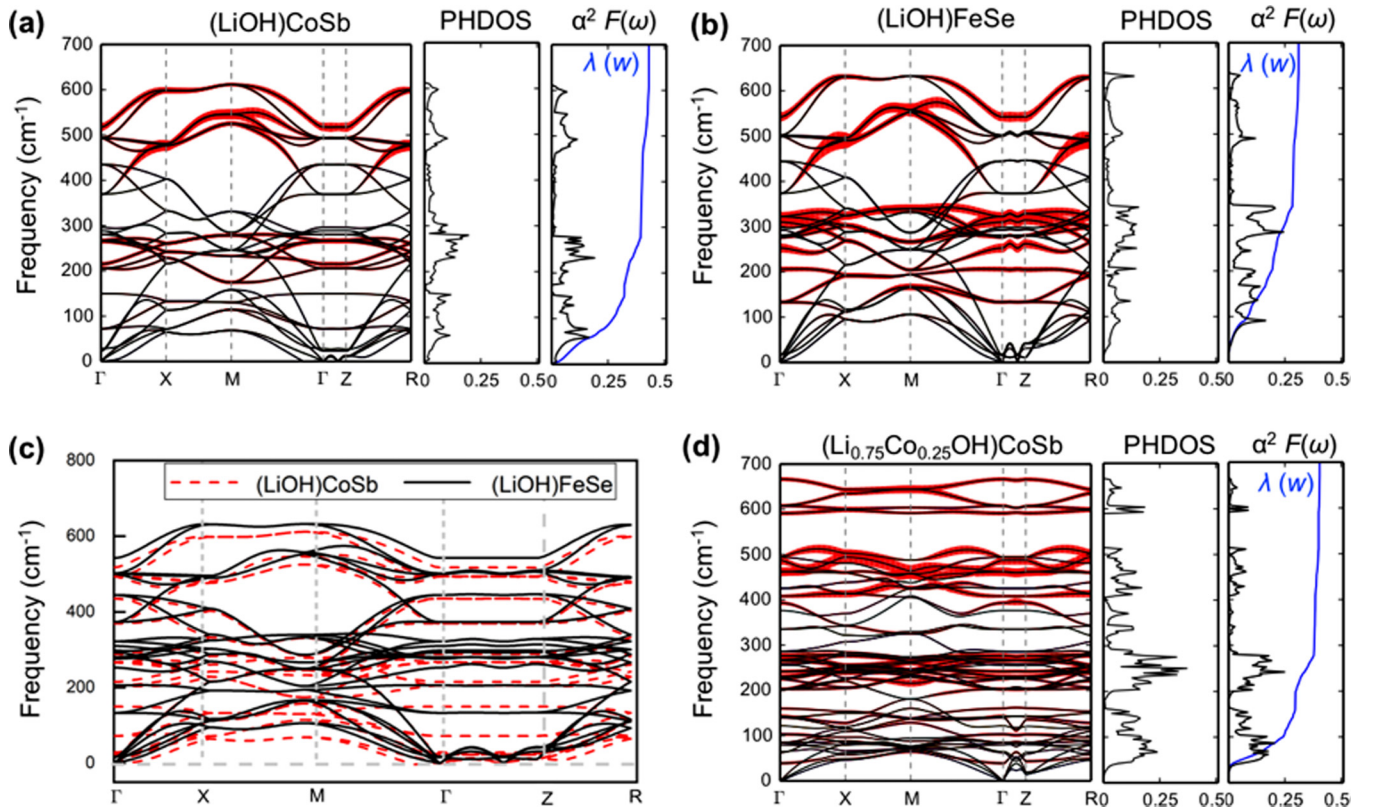
FIG. 3. Phonon dispersion relation, phonon density of states (PHDOS), Eliashberg function $\alpha^2 F(\omega)$ (black), and the cumulative electron-phonon coupling $\lambda(\omega)$ (blue) for (a) (LiOH)CoSb and (b) (LiOH)FeSe, respectively. The magnitudes of the phonon linewidth are indicated by the sizes of the red error bars. (c) Comparison of the phonon dispersions of both (LiOH)CoSb and (LiOH)FeSe superlattice structures. The dashed (red) and solid (black) lines represent the phonon spectra of (LiOH)CoSb and (LiOH)FeSe respectively, indicating the phonon softening for (LiOH)CoSb. (d) Same as in (a) or (b), but for $(Li_{0.75}Co_{0.25}OH)CoSb$.

especially their ability to harbor high T_c [13–16,73–77]. We construct an electron-doped superlattice structure of $(Li_{0.75}Co_{0.25}OH)CoSb$ by substituting 25% of Li with Co in the spacer layers of (Li,Co,OH), as shown in Figs. 1(a) and 5(b). As presented in Table I, $(Li_{0.75}Co_{0.25}OH)CoSb$ possesses lattice constants of $a = 3.95\,Å$ and $c = 10.07\,Å$ with SOC effects included, and a cohesive energy of 0.28 eV/f.u, exhibiting a more compact cell size and stronger interlayer couplings than that of (LiOH)CoSb. These results reveal that the superlattice structure of $(Li_{1-x}Co_xOH)CoSb$ has been further stabilized by electron doping. As shown in Fig. 3(d), the phonon spectrum of $(Li_{0.75}Co_{0.25}OH)CoSb$ possesses no imaginary frequency, indicating that the system stays dynamically stable. Our AIMD simulations on $(Li_{0.75}Co_{0.25}OH)CoSb$ at 100 K and up to 8 ps further demonstrate that the system is thermodynamically stable as well, as shown in Fig. 1(d).

We then investigate the detailed nature of interlayer charge transfer in $(Li_{1-x}Co_xOH)CoSb$ with or without Co doping in the spacer layers. Figure 4 presents the plane-averaged charge density differences $(\Delta \rho_z)$ along the c axis for $(Li_{1-x}Co_xOH)CoSb$ in comparison with that of $(Li_{1-x}Fe_x)OHFeSe$. As shown in Fig. 4(a), when the electron-doped $(Li_{0.75}Co_{0.25}OH)$ spacer layers and the CoSb layers merge into the $(Li_{0.75}Co_{0.25}OH)CoSb$ superlattice structure, an electron-deletion region is formed around the spacer layers, and this amount of electron charge has been mostly trans-

ferred to the interfacial region close to the CoSb layers. In contrast, the undoped (LiOH)CoSb system possesses no such significant charge transfer, as shown in Fig. 4(b). To further obtain the doping levels, we integrate the electron injection ρ_I within the region of CoSb, shown as the grey shaded areas in Figs. 4(a) and 4(b) (the boundaries between the spacer and CoSb layers are located at the places where the $\Delta \rho_z$ changes sign). The electron injection ρ_I is calculated to be 0.06 e/f.u. for $(Li_{0.75}Co_{0.25}OH)CoSb$, while it is only 0.02 e/f.u. for the undoped (LiOH)CoSb system. As shown in Figs. 4(c) and 4(d), these charge-carrier transfer results are also comparable to that of the $(Li_{1-x}Fe_xOH)FeSe$ systems ($\rho_I = 0.06\,e/$f.u at $x = 0.25$).

We now investigate the superconducting properties of the electron-doped $(Li_{0.75}Co_{0.25}OH)CoSb$ system, again using the EPC strength as a quantitative indicator. As shown in Fig. 3(d), the EPC strength λ of the electron-doped $(Li_{0.75}Co_{0.25}OH)CoSb$ system is 0.41 comparable to that of (LiOH)CoSb ($\lambda = 0.43$). On the other hand, the calculated logarithmically averaged phonon frequency ω_{log} [see Eq. (3) in the Methods section] of $(Li_{0.75}Co_{0.25}OH)CoSb$ is 154.8 K, substantially higher than that of (LiOH)CoSb ($\omega_{log} = 107.1$ K). Therefore, by using the McMillian-Allen-Dynes parametrized Eliashberg equation (with $\mu^* = 0.1$), the T_c of $(Li_{0.75}Co_{0.25}OH)CoSb$ is estimated to be 0.85 K, which is ~ 1.4 times higher than that of (LiOH)CoSb ($T_c \sim 0.62$ K). Qualitatively, this higher T_c of $(Li_{0.75}Co_{0.25}OH)CoSb$ can be
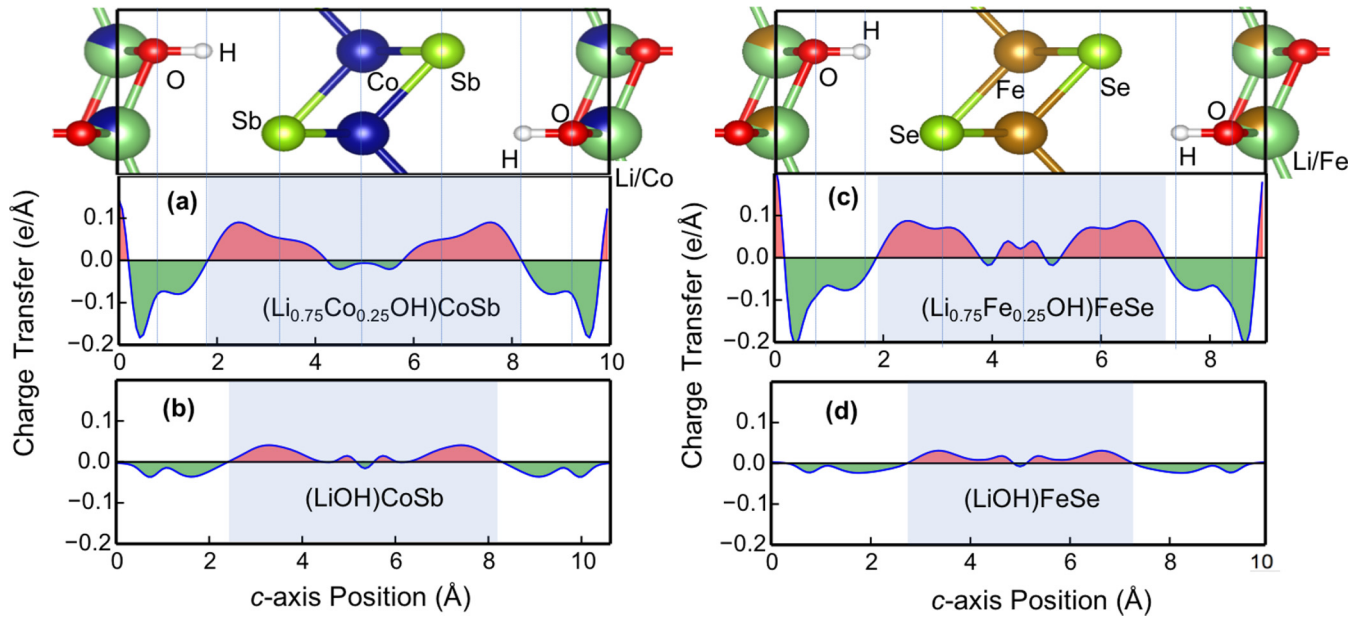
FIG. 4. Charge density difference distributions of $(Li_{1-x}Co_xOH)CoSb$ with (a) $x = 0.25$ and (b) $x = 0$, respectively. (c), (d) Same as (a) and (b) respectively, but for $(Li_{1-x}Fe_xOH)FeSe$. The red and green areas indicate electron accumulation and depletion region, respectively.

attributed to two aspects: first, through electron doping, extra charge carriers will be injected into the CoSb superconducting layers, which may increase the possibilities for electron pairing around the Fermi level and compensate the phonon hardening effects on λ [see Eqs. (1)–(3) in the Methods section]; second, the doping of Co in the spacer layers increases the interlayer binding energies, which may stiffen the superlattice structures and introduce new phonon modes for possible phonon-mediated electron pairing processes. These results indicate that the T_c of $(Li_{1-x}Co_xOH)CoSb$ can be enhanced by electron doping effects.

On the other hand, as mentioned above, the DFPT calculations can substantially underestimate the EPC and T_c of FeSe and related systems [27,69–71], since DFT cannot reliably describe the strong correlation effects associated with the $3d$ electrons. For example, a recent study has shown that the dynamical mean-field theory (DMFT)+DFT methods can improve the agreement between theory and experiment in the electron-phonon coupling strength of bulk FeSe by as large as about one order of magnitude of enhancement [69]. However, full-spectrum calculations of the superconducting properties of FeSe and related within the DMFT+DFT formalism are presently still too demanding computationally.

Even though the dominant mechanisms for the high-T_c superconductivity in FeSe-based superconductors are still under debate, recent studies have pointed to several crucial ingredients. First, the FeSe monolayer stands out as the distinct building block for constructing various high-T_c superconductors [7]. Second, by stacking into superlattice structures or placing on proper substrates, the superconductivity of the FeSe monolayers can be substantially enhanced [8–14,78]. Third, significant charge transfer into the FeSe layers is indispensable in achieving high T_c's in $(Li_{1-x}Fe_xOH)FeSe$ [13–16,73] and other FeSe-based superconductors [74–77]. Based on the present study, the $(Li_{1-x}Co_xOH)CoSb$ systems possess all these essential ingredients, thereby strongly

favoring the systems to serve as a highly appealing platform for realizing high-T_c superconductivity beyond the FeSe-based superconductors.

D. Topological properties of $(Li_{1-x}Co_xOH)CoSb$

We next demonstrate that the electronic structure of (LiOH)CoSb is topologically nontrivial, as characterized collectively by a band inversion along the Γ-Z path of the Brillouin zone (BZ), odd Z_2 invariants, and detailed surface-state calculations. As discussed in Sec. III A, due to the relatively strong SOC effects of Sb, the lattice constants of (LiOH)CoSb have been substantially changed (see Table I). Therefore, it is important to investigate the topological properties of the corresponding system within the fully relaxed geometry. Figures 2(d) and 2(e) present the projected band structures of (LiOH)CoSb in the fully relaxed lattice constants without or with the SOC effects, respectively. As shown in Fig. 2(d), without the SOC effects, the CoSb layer contributes the twofold degenerate flat bands with d_{xz}/d_{yz} orbitals of Co, and a nondegenerate band with considerable dispersion along the Γ-Z direction is mainly contributed from the p_z orbitals of Sb. The remaining two nondegenerate flat bands are mainly contributed from the $d_{x^2-y^2}$ and d_{xy} orbitals along the Γ-Z path. Upon inclusion of SOC, the twofold degenerate d_{xz}/d_{yz} bands split along the Γ-Z path, with one of them shifting downwards and intersecting with the upward-shifting p_z band. As a result, a band inversion occurs along the Γ-Z path by interchanging the relative positions of the d_{xz}/d_{yz} and p_z bands, and two SOC gaps of 1.4 and 9 meV are opened along the Γ-Z path and Γ-M path, respectively.

To further confirm the topological nature of (LiOH)CoSb, we calculate the Z_2 topological invariant through the evolution of Wannier charge centers [47] by assuming a "curved chemical potential," namely the magenta dashed line in Fig. 2(e). We find that Z_2 for the corresponding system is 1, thereby

substantiating the nontrivial topology. Moreover, we can also examine the band characters of the corresponding system by using the method of EBRs (see the Methods section). After a careful scan, we find that the band characters cannot be written as either a sum or a difference of the EBRs in the space group, implying a nontrivial topology with topological indices $Z_{2w,1} = 0$, $Z_{2w,2} = 0$, $Z_{2w,3} = 0$, $Z_4 = 3$ and $Z_2 = 1$. For the symmetry group 129, the topological indices Z_4 and $Z_{2w,i=1,2,3}$ identify the strong or weak topological nature of the system [79]. The odd value of the former gives the strong whereas the latter gives the weak topological nature, respectively.

Based on the above collective analyses, we conclude that (LiOH)CoSb shares the same topological characters as strong topological insulators with the $\mathbf{Z_2}$ invariant $(v_0; v_1, v_2, v_3) = (1; 000)$. Correspondingly, the TSSs are expected to appear on the surfaces of (LiOH)CoSb according to the bulk-boundary correspondence. Indeed, as shown in Fig. 2(f), by calculating the surface Green's function of a semi-infinite slab system, we find that the local density of states (LDOS) on the (100) surface of (LiOH)CoSb exhibits the TSSs along the $\bar{M}$-$\bar{\Gamma}$-$\bar{M}$ path which are well separated from the bulk states. These results agree with the Z_2 invariant calculations, confirming again the nontrivial topological nature of (LiOH)CoSb.

In this system, although the band inversion occurs at about 0.6 eV above the Fermi level [Fig. 2(e)], our surface-state calculations show that the topological surface states cross the Fermi level along the $\bar{M}$-$\bar{\Gamma}$ path [Fig. 2(f)]. Such topological surface states can hold spin-momentum-locked spin textures [80]. Below the superconducting critical temperature, the spin-momentum-locked surface states around the Fermi level will open a superconducting gap, and the resulting superconductivity at the surface can be viewed as possessing an equivalent $p_x + ip_y$ symmetry [81].

Next, we analyze how the band topology of (LiOH)CoSb behaves under electron doping. To explore the topological phase in $(Li_{0.75}Co_{0.25}OH)CoSb$, we calculate the eigenvalues at the high-symmetry k points of a space group 129 and examine the band characters by the EBRs method as an initial screening. Surprisingly, we find that (LiOH)CoSb, a topologically nontrivial parent material, undergoes a phase transition upon such a high doping concentration of $x = 0.25$, close to that of the high-T_c $(Li_{1-x}Fe_xOH)FeSe$ systems. The phase transition in the corresponding system is most likely due to the crossing twice of the p_z band in the whole BZ, as an even number of band crossings may correspond to either a weak topological phase or topologically trivial phase [82,83]. In this regard, we note that although doping is mandatory in order to enhance the T_c in FeSe-based superconductors [6,13,14], T_c can also be significantly enhanced upon pressure without heavy doping [84]. For example, we speculate that uniaxial pressure can not only preserve the nontrivial topology to be intact in the (LiOH)CoSb system, but may also substantially enhance the charge transfer and high T_c. Detailed results are to be reported in a forthcoming systematic study of pressure effects on the high-T_c materials. In the present work, the topological properties for the doped system are studied based on the EBRs method alone, while more systematic computations with the inclusion of a higher level of many-body effects need to be performed at different concentrations

of x to possibly identify a clear boundary between the two phases. The important emphasis made here is that the clean system of (LiOH)CoSb is a much more highly desirable candidate system for reaching topological superconductivity, with more readily detectable topological excitations such as the Majorana zero modes.

E. Magnetic properties of $(Li_{1-x}Co_xOH)CoSb$

For FeSe/STO and $(Li_{1-x}Fe_xOH)FeSe$, aside from the dominant superconductivity enhancement mechanisms due to the substrate or the spacer layers, even less is known about the intrinsic pairing mechanisms in the FeSe monolayers. Earlier theoretical studies emphasized antiferromagnetic spin fluctuations to be potentially dominating [23,24]. More recently, the EPC has been increasingly recognized as likely the dominant microscopic origin of superconductivity in the FeSe monolayers with variable T_c's [26,28,29]. Here, because of the different numbers of d valence electrons in the superconducting layers, $(Li_{1-x}Co_xOH)CoSb$ may exhibit physical properties different from $(Li_{1-x}Fe_xOH)FeSe$, especially surrounding magnetism.

To explore this point, we consider four magnetic configurations for both the superconducting CoSb layers and the $(Li_{0.75}Co_{0.25}OH)$ spacer layers of $(Li_{0.75}Co_{0.25}OH)CoSb$, in comparison with that of $(Li_{0.75}Fe_{0.25}OH)FeSe$. These include the nonmagnetic (NM), ferromagnetic (FM), Néel antiferromagnetic (NAFM), and collinear antiferromagnetic (CAFM) phases, as shown in Figs. 5(a) and 5(b). Our calculations without an on-site Hubbard U show that the ground-state (GS) configurations in the spacer layers of both $(Li_{0.75}Co_{0.25}OH)$ and $(Li_{0.75}Fe_{0.25}OH)$ are CAFM, while the GSs for the superconducting layers of these systems are distinctly different, with NM for the CoSb layers and CAFM for the FeSe layers, respectively. We further use an on-site Hubbard U as the empirical parameter to describe the correlation effects of the $3d$ electrons. As shown in Figs. 5(c) and 5(d), the magnetic moments M in different magnetic configurations for the superconducting layers of CoSb and FeSe are displayed as a function of U, together with the relative energies ΔE defined as $\Delta E = E - E_{CAFM}$, where E and E_{CAFM} are the total energies of a given magnetic and CAFM configuration, respectively. At $U = 0$ eV, the GS for the CoSb layers is NM, with $M = 0$; in contrast, the GS for the FeSe layers is CAFM, with $M = 2 \mu_B/Fe$. Moreover, for the CoSb layers, M is finite only when $U > 2$ eV, and saturates at $\sim 2 \mu_B/Co$, while for the FeSe layers, M is always finite and varies within $1.8 \sim 3.2 \mu_B/Fe$, depending on the specific magnetic configurations. On the other hand, at $U = 0$ eV, the GSs for the spacer layers of both $(Li_{0.75}Co_{0.25}OH)$ and $(Li_{0.75}Fe_{0.25}OH)$ are CAFM, with magnetic moments of $M = 2.4 \mu_B/Co$ and $M = 3.5 \mu_B/Fe$, respectively. Moreover, the dependencies of M on U for the spacer layers of both $(Li_{0.75}Co_{0.25}OH)$ and $(Li_{0.75}Fe_{0.25}OH)$ are relatively weak, as shown in Figs. 5(c) and 5(d). These major differences in the magnetic properties of $(Li_{0.75}Co_{0.25}OH)CoSb$ and $(Li_{0.75}Fe_{0.25}OH)FeSe$ can be qualitatively attributed to the overall more delocalized nature of the electrons in CoSb than that in FeSe [37], and may provide a crucial angle to elucidate the dominant microscopic mechanisms of superconductivity in these and related systems.
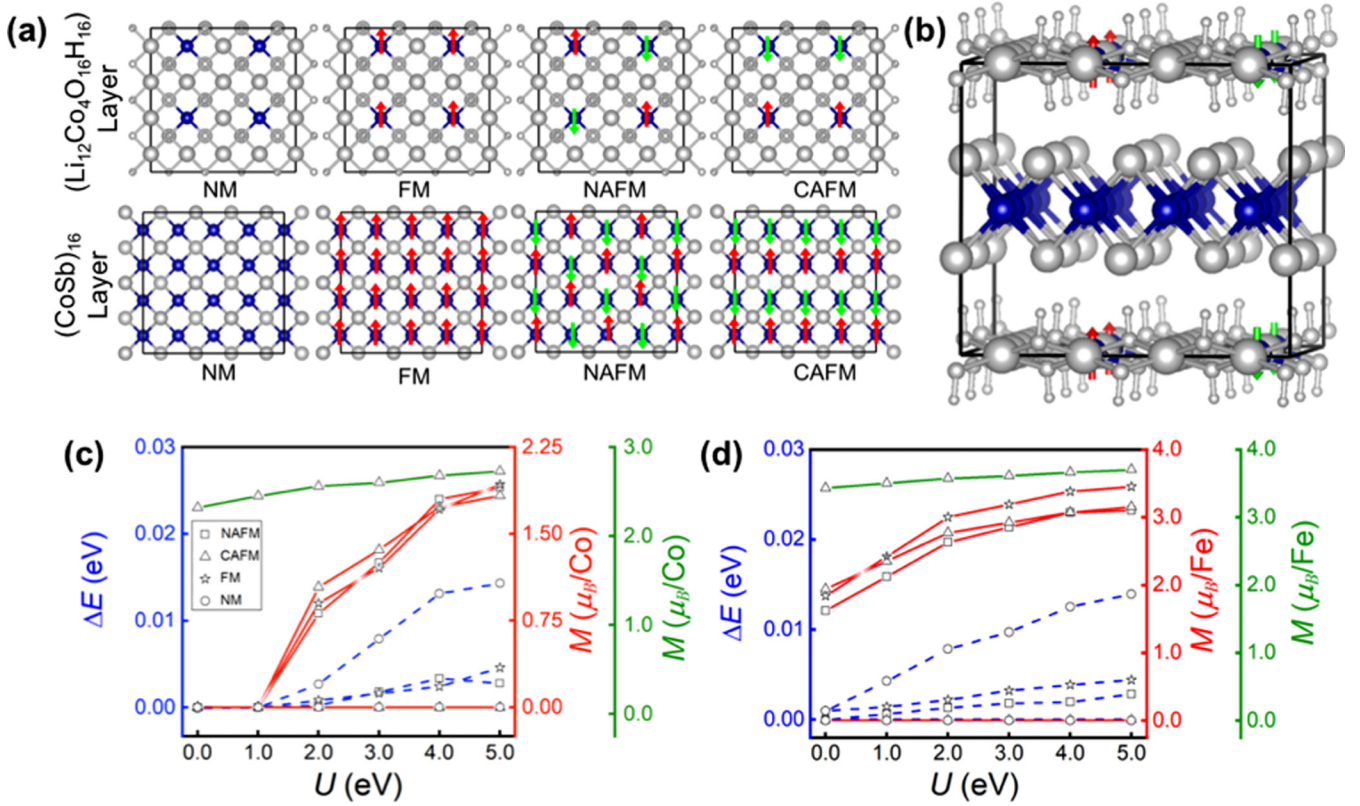
FIG. 5. (a) The magnetic orders of the $(Li_{0.75}Co_{0.25}OH)$ spacer layers (top panel) and the CoSb superconducting layers (lower panel) calculated to estimate the ground state of $(Li_{0.75}Co_{0.25}OH)CoSb$. (b) Ground-state configuration of $(Li_{0.75}Co_{0.25}OH)CoSb$ with CAFM in the $(Li_{0.75}Co_{0.25}OH)$ spacer layers and NM in the CoSb layers. The Co atoms are labeled in blue and the opposite spin directions are shown with the red and green arrows, respectively. (c) Dependencies of the magnetic moment M for the CoSb layer (solid red), $(Li_{0.75}Co_{0.25}OH)$ layer (solid dark green), and ΔE (dotted blue) as a function of the on-site Hubbard U for the $(Li_{0.75}Co_{0.25}OH)CoSb$ system. (d) Same as (c), but for the $(Li_{0.75}Fe_{0.25}OH)FeSe$ system.

IV. DISCUSSION

In this work, we choose the nonmagnetic states of $(Li_{1-x}Co_xOH)CoSb$ for studying their topological and superconducting properties, for two reasons. First, our calculations show that the superconducting layers (CoSb) of $(Li_{1-x}Co_xOH)CoSb$ possess only a nonmagnetic state as long as the Hubbard $U < 2\,\text{eV}$ (namely, with zero magnetic moment per Co atom). When $U > 2\,\text{eV}$, the CoSb layers of $(Li_{1-x}Co_xOH)CoSb$ also show a much weaker tendency towards magnetization (namely still with a much smaller magnetic moment per Co atom) than that of the FeSe counterparts in $(Li_{1-x}Fe_xOH)FeSe$. Second, since the electronic states within the energy window $[-1, 1\,\text{eV}]$ of $(Li_{1-x}Co_xOH)CoSb$ are primarily contributed by the CoSb layers, the magnetic states of the spacer layers $(Li_{1-x}Co_xOH)$ would hardly affect the band structures around the Fermi levels of $(Li_{1-x}Co_xOH)CoSb$, as also demonstrated previously in a related study of the $(Li_{1-x}Fe_xOH)FeSe$ superlattices [85].

The latest developments on understanding the microscopic superconducting mechanisms of FeSe-based superconductors are mostly centered on two aspects, namely the magnetism driven spin fluctuations [23,24] and EPC [3,25–29]. The coexistence of (anti)magnetism and high-T_c superconductivity has been observed in $(Li_{1-x}Fe_xOH)FeSe$ by NMR experiments [13,14]. In this work, we have shown that $(Li_{1-x}Co_xOH)CoSb$

exhibits distinctly different magnetic properties from that of $(Li_{1-x}Fe_xOH)FeSe$, while the EPC-based superconducting properties of these two systems are comparable. These findings should provide a crucial angle to elucidate the dominant microscopic mechanisms of superconductivity in these and related systems. In particular, if $(Li_{1-x}Co_xOH)CoSb$ is definitively confirmed to be a high-T_c system, it will provide a key piece of evidence to exclude the spin-fluctuation mechanism as the dominant one. In contrast, if $(Li_{1-x}Co_xOH)CoSb$ is not a high-T_c system, the finding should offer complementary support to the spin-fluctuation mechanism. Such insights may lead to distinct differentiation between the dominant competing mechanisms of superconductivity.

Because of the relatively weak SOC effects in FeSe, extrinsic doping may be mandatory for obtaining the nontrivial topological properties in FeSe-based superconductors [4–6,17,18]. Such doping could induce unwanted defects and hinder the detection and manipulation of Majorana zero modes. In this regard, $(Li_{1-x}Fe_xOH)FeSe$ was proposed to be a relatively clean platform for realizing topological superconductivity, as it at least does not need to dope Te in the superconducting layers [6]. On the other hand, an appropriate amount of electron doping could also be helpful for inducing the surface phase transition from the normal superconducting state to the topological superconducting state [19], although the microscopic pairing and topological

superconducting mechanisms in these systems are still under debate [86]. Here we have shown that (LiOH)CoSb possesses intrinsically nontrivial topological properties without the need of extrinsic doping in either the superconducting or the spacer layers, which should provide a more ideal and cleaner platform for exploring topological superconductivity. In addition, with the application of proper pressure, high transition temperatures of superconductivity can also be expected.

In order to verify experimentally the strong and innovative predictions made here on $(Li_{1-x}Co_xOH)CoSb$, one should notice that the preferred bulk structure of CoSb is not layered, distinctly different from that of the PbO-type layered structure of bulk FeSe. Therefore, the methodologies used in the synthesis of $(Li_{1-x}Fe_xOH)FeSe$, such as the hydrothermal reaction methods [13,14], may demand more optimized fine tuning when applied to the fabrication of these CoSb-based superlattice structures. Recently, monolayered CoSb films with different symmetries have been successfully synthesized on $SrTiO_3$ (STO) substrates by molecular-beam epitaxy [38,39] and in La-intercalated bulk structure of $CoSb_2$ by an arc-melting method [40], confirming that the CoSb monolayers can indeed exist in completely different forms from its bulk phase, especially if properly supported and through carefully devised kinetic growth pathways. If future experimental studies further confirm the other vital manifestations of the topological superconductors in the CoSb-based family [37], we would be empowered with a different materials platform in developing innovative architectures for topological quantum computation.

V. CONCLUSIONS

In conclusion, we have identified a chemically isovalent and structurally identical counterpart of $(Li_{1-x}Fe_xOH)FeSe$, namely, $(Li_{1-x}Co_xOH)CoSb$, which is an attractive candidate to harbor high-T_c superconductivity beyond the well-established Cu- and Fe-based superconducting families. Our comprehensive studies have shown that $(Li_{1-x}Co_xOH)CoSb$ ($x = 0$ or 0.25) are energetically, dynamically, and thermodynamically stable. Furthermore, $(Li_{1-x}Co_xOH)CoSb$ possess

EPC properties superior to $(Li_{1-x}Fe_xOH)FeSe$, as well as substantial interlayer charge transfer, strongly favoring the system to be an appealing candidate for realizing high-T_c superconductivity. More strikingly, we revealed that (LiOH)CoSb is topologically nontrivial even without any extrinsic doping in either the superconducting layers or the spacer layers, in sharp contrast to its counterpart of $(Li_{1-x}Fe_xOH)FeSe$, which is trivial in the undoped case. Therefore, the present study offers a cleaner candidate system for realizing topological superconductivity. Finally, we showed that $(Li_{1-x}Co_xOH)CoSb$ exhibits overall weaker elemental magnetic moments than $(Li_{1-x}Fe_xOH)FeSe$, which may provide a different angle for elucidating the dominant microscopic mechanisms of superconductivity in these and related systems. Considering the rapid developments in ingenious synthesis of quantum materials in recent years, we are optimistic that $(Li_{1-x}Co_xOH)CoSb$ will be fabricated experimentally in the near future, and will offer opportunities in fundamental and applied superconductivity research.

[1] J. Paglione and R. L. Greene, High-temperature superconductivity in iron-based materials, Nat. Phys. **6**, 645 (2010).

[2] A. I. Coldea and M. D. Watson, The Key Ingredients of the Electronic Structure of FeSe, Annu. Rev. Condens. Matter Phys. **9**, 125 (2018).

[3] D.-H. Lee, Routes to high-temperature superconductivity: A lesson from $FeSe/SrTiO_3$, Annu. Rev. Condens. Matter Phys. **9**, 261 (2018).

[4] P. Zhang, K. Yaji, T. Hashimoto, Y. Ota, T. Kondo, K. Okazaki, Z. Wang, J. Wen, G. D. Gu, H. Ding, and S. Shin, Observation of topological superconductivity on the surface of an iron-based superconductor, Science **360**, 182 (2018).

[5] D. Wang, L. Kong, P. Fan, H. Chen, S. Zhu, W. Liu, L. Cao, Y. Sun, S. Du, J. Schneeloch, R. Zhong, G. Gu, L. Fu, H. Ding, and H.-J. Gao, Evidence for Majorana bound states in an iron-based superconductor, Science **362**, 333 (2018).

[6] Q. Liu, C. Chen, T. Zhang, R. Peng, Y.-J. Yan, C.-H.-P. Wen, X. Lou, Y.-L. Huang, J.-P. Tian, X.-L. Dong, G.-W. Wang, W.-C. Bao, Q.-H. Wang, Z.-P. Yin, Z.-X. Zhao, and D.-L. Feng, Robust and Clean Majorana Zero Mode in the Vortex Core of High-Temperature Superconductor ($Li_{0.84}Fe_{0.16}$) OHFeSe, Phys. Rev. X **8**, 041056 (2018).

[7] F.-C. Hsu, J.-Y. Luo, K.-W. Yeh, T.-K. Chen, T.-W. Huang, P. M. Wu, Y.-C. Lee, Y.-L. Huang, Y.-Y. Chu, D.-C. Yan, and M.-K. Wu, Superconductivity in the PbO-type structure α-FeSe, Proc. Natl. Acad. Sci. USA **105**, 14262 (2008).

[8] Q.-Y. Wang, Z. Li, W.-H. Zhang, Z.-C. Zhang, J.-S. Zhang, W. Li, H. Ding, Y.-B. Ou, P. Deng, K. Chang, J. Wen, C.-L. Song, K. He, J.-F. Jia, S.-H. Ji, Y.-Y. Wang, L.-L. Wang, X. Chen, X.-C. Ma, and Q.-K. Xue, Interface-induced high-temperature superconductivity in single unit-cell FeSe films on $SrTiO_3$, Chin. Phys. Lett. **29**, 037402 (2012).

[9] R. Peng, H. C. Xu, S. Y. Tan, H. Y. Cao, M. Xia, X. P. Shen, Z. C. Huang, C. H. Wen, Q. Song, T. Zhang, B. P. Xie, X. G. Gong, and D. L. Feng, Tuning the band structure and superconductivity in single-layer FeSe by interface engineering, Nat. Commun. **5**, 5044 (2014).

[10] H. Ding, Y. F. Lv, K. Zhao, W. L. Wang, L. Wang, C. L. Song, X. Chen, X. C. Ma, and Q. K. Xue, High-Temperature Superconductivity in Single-Unit-Cell FeSe Films on Anatase TiO_2(001), Phys. Rev. Lett. **117**, 067001 (2016).

[11] J. Guo, S. Jin, G. Wang, S. Wang, K. Zhu, T. Zhou, M. He, and X. Chen, Superconductivity in the iron selenide $K_xFe_2Se_2$ ($0 \leqslant x \leqslant 1.0$), Phys. Rev. B **82**, 180520(R) (2010).

[12] M. Burrard-Lucas, D. G. Free, S. J. Sedlmaier, J. D. Wright, S. J. Cassidy, Y. Hara, A. J. Corkett, T. Lancaster, P. J. Baker, S. J. Blundell, and S. J. Clarke, Enhancement of the superconducting transition temperature of FeSe by intercalation of a molecular spacer layer, Nat. Mater. **12**, 15 (2013).

[13] X. F. Lu, N. Z. Wang, H. Wu, Y. P. Wu, D. Zhao, X. Z. Zeng, X. G. Luo, T. Wu, W. Bao, G. H. Zhang, F. Q. Huang, Q. Z. Huang, and X. H. Chen, Coexistence of superconductivity and antiferromagnetism in ($Li_{0.8}Fe_{0.2}$)OHFeSe, Nat. Mater. **14**, 325 (2015).

[14] U. Pachmayr, F. Nitsche, H. Luetkens, S. Kamusella, F. Bruckner, R. Sarkar, H. H. Klauss, and D. Johrendt, Coexistence of 3d-ferromagnetism and superconductivity in [($Li_{1-x}Fe_x$)OH]($Fe_{1-y}Li_y$)Se, Angew. Chem. Int. Ed. **54**, 293 (2015).

[15] X. H. Niu, R. Peng, H. C. Xu, Y. J. Yan, J. Jiang, D. F. Xu, T. L. Yu, Q. Song, Z. C. Huang, Y. X. Wang, B. P. Xie, X. F. Lu, N. Z. Wang, X. H. Chen, Z. Sun, and D. L. Feng, Surface electronic structure and isotropic superconducting gap in ($Li_{0.8}Fe_{0.2}$) OHFeSe, Phys. Rev. B **92**, 060504(R) (2015).

[16] L. Zhao, A. Liang, D. Yuan, Y. Hu, D. Liu, J. Huang *et al.*, Common electronic origin of superconductivity in (Li,Fe)OHFeSe bulk superconductor and single-layer $FeSe/SrTiO_3$ films, Nat. Commun. **7**, 10608 (2016).

[17] Z. Wang, P. Zhang, G. Xu, L. K. Zeng, H. Miao, X. Xu, T. Qian, H. Weng, P. Richard, A. V. Fedorov, H. Ding, X. Dai, and Z. Fang, Topological nature of the $FeSe_{0.5}Te_{0.5}$ superconductor, Phys. Rev. B **92**, 115119 (2015).

[18] X. Wu, S. Qin, Y. Liang, H. Fan, and J. Hu, Topological characters in $Fe(Te_{1-x}Se_x)$ thin films, Phys. Rev. B **93**, 115129 (2016).

[19] G. Xu, B. Lian, P. Tang, X.-L. Qi, and S.-C. Zhang, Topological Superconductivity on the Surface of Fe-Based Superconductors, Phys. Rev. Lett. **117**, 047001 (2016).

[20] V. Mourik, K. Zuo, S. M. Frolov, S. R. Plissard, E. P. A. M. Bakkers, and L. P. Kouwenhoven, Signatures of majorana fermions in hybrid superconductor-semiconductor nanowire devices, Science **336**, 1003 (2012).

[21] S.-Y. Xu, N. Alidoust, I. Belopolski, A. Richardella, C. Liu, M. Neupane *et al.*, Momentum-space imaging of Cooper pairing in a half-Dirac-gas topological superconductor, Nat. Phys. **10**, 943 (2014).

[22] H.-H. Sun, K.-W. Zhang, L.-H. Hu, C. Li, G.-Y. Wang, H.-Y. Ma, Z.-A. Xu, C. L. Gao, D.-D. Guan, Y.-Y. Li, C. Liu, D. Qian, Y. Zhou, L. Fu, S.-C. Li, F.-C. Zhang, and J.-F. Jia, Majorana Zero Mode Detected with Spin Selective Andreev Reflection in the Vortex of a Topological Superconductor, Phys. Rev. Lett. **116**, 257003 (2016).

[23] P. J. Hirschfeld, M. M. Korshunov, and I. I. Mazin, Gap symmetry and structure of Fe-based superconductors, Rep. Prog. Phys. **74**, 124508 (2011).

[24] D. J. Scalapino, A common thread: The pairing interaction for unconventional superconductors, Rev. Mod. Phys. **84**, 1383 (2012).

[25] J. J. Lee, F. T. Schmitt, R. G. Moore, S. Johnston, Y. T. Cui, W. Li, M. Yi, Z. K. Liu, M. Hashimoto, Y. Zhang, D. H. Lu, T. P. Devereaux, D. H. Lee, and Z. X. Shen, Interfacial mode coupling as the origin of the enhancement of T_c in FeSe films on $SrTiO_3$, Nature (London) **515**, 245 (2014).

[26] S. Coh, M. L. Cohen, and S. G. Louie, Large electron-phonon interactions from FeSe phonons in a monolayer, New J. Phys. **17**, 073027 (2015).

[27] S. Gerber, S. L. Yang, D. Zhu, H. Soifer, J. A. Sobota, S. Rebec *et al.*, Femtosecond electron-phonon lock-in by photoemission and x-ray free-electron laser, Science **357**, 71 (2017).

[28] S. Zhang, T. Wei, J. Guan, Q. Zhu, W. Qin, W. Wang, J. Zhang, E. W. Plummer, X. Zhu, Z. Zhang, and J. Guo, Enhanced Superconducting State in $FeSe/SrTiO_3$ by a Dynamic Interfacial Polaron Mechanism, Phys. Rev. Lett. **122**, 066802 (2019).

[29] Y. L. Huang, J. Yuan, T. Wei, Z. P. Feng, W. Hu, W. Qin *et al.*, Tuning the intricate multi-fluidity nature of ($Li_{1-x}Fe_x$OH)FeSe films for optimally enhanced superconductivity (unpublished).

[30] L. Kong, S. Zhu, M. Papaj, H. Chen, L. Cao, H. Isobe *et al.*, Half-integer level shift of vortex bound states in an iron-based superconductor, Nat. Phys. **15**, 1181 (2019).

[31] S. Zhu, L. Kong, L. Cao, H. Chen, M. Papaj, S. Du *et al.*, Nearly quantized conductance plateau of vortex zero mode in an iron-based superconductor, Science **367**, 189 (2020).

[32] C. Chen, K. Jiang, Y. Zhang, C. Liu, Y. Liu, Z. Wang, and J. Wang, Atomic line defects and zero-energy end states in monolayer Fe(Te,Se) high-temperature superconductors, Nat. Phys. **16**, 536 (2020).

[33] C. Chen, Q. Liu, T. Z. Zhang, D. Li, P. P. Shen, X. L. Dong, Z. X. Zhao, T. Zhang, and D. L. Feng, Quantized conductance of majorana zero mode in the vortex of the topological superconductor ($Li_{0.84}Fe_{0.16}$)OHFeSe, Chin. Phys. Lett. **36**, 057403 (2019).

[34] H. Hosono, K. Tanabe, E. Takayama-Muromachi, H. Kageyama, S. Yamanaka, H. Kumakura, M. Nohara, H. Hiramatsu, and S. Fujitsu, Exploration of new superconductors and functional materials, and fabrication of superconducting tapes and wires of iron pnictides, Sci. Technol. Adv. Mater. **16**, 033503 (2015).

[35] Z. Zhu, X. Cai, S. Yi, J. Chen, Y. Dai, C. Niu, Z. Guo, M. Xie, F. Liu, J. H. Cho, Y. Jia, and Z. Zhang, Multivalency-Driven Formation of Te-Based Monolayer Materials: A Combined First-Principles and Experimental study, Phys. Rev. Lett. **119**, 106101 (2017).

[36] M. C. Lucking, W. Xie, D.-H. Choe, D. West, T.-M. Lu, and S. B. Zhang, Traditional Semiconductors in the Two-Dimensional Limit, Phys. Rev. Lett. **120**, 086101 (2018).

[37] W. Ding, J. Zeng, W. Qin, P. Cui, and Z. Zhang, Exploring High Transition Temperature Superconductivity in a Freestanding or $SrTiO_3$-Supported CoSb Monolayer, Phys. Rev. Lett. **124**, 027002 (2020).

[38] C. Ding, G. Gong, Y. Liu, F. Zheng, Z. Zhang, H. Yang, Z. Li, Y. Xing, J. Ge, K. He, W. Li, P. Zhang, J. Wang, L. Wang, and Q. K. Xue, Signature of superconductivity in orthorhombic

CoSb monolayer films on $SrTiO_3(001)$, ACS Nano **13**, 10434 (2019).

[39] H. Zhang and C. Zeng (private communications).

[40] M. Zou, J. Chu, H. Zhang, T. Yuan, P. Cheng, W. Jin, D. Jiang, X. Xu, W. Yu, Z. An, X. Wei, G. Mu, and W. Li, Evidence for ferromagnetic order in the CoSb layer of $LaCoSb_2$, Phys. Rev. B **101**, 155138 (2020).

[41] G. Kresse and J. Furthmüller, Efficient iterative schemes for ab initio total-energy calculations using a plane-wave basis set, Phys. Rev. B **54**, 11169 (1996).

[42] P. E. Blochl, Projector augmented-wave method, Phys. Rev. B **50**, 17953 (1994).

[43] J. P. Perdew, K. Burke, and M. Ernzerhof, Generalized Gradient Approximation made Simple, Phys. Rev. Lett. **77**, 3865 (1996).

[44] K. Lee, É. D. Murray, L. Kong, B. I. Lundqvist, and D. C. Langreth, Higher-accuracy van der Waals density functional, Phys. Rev. B **82**, 081101(R) (2010).

[45] S. L. Dudarev, G. A. Botton, S. Y. Savrasov, C. J. Humphreys, and A. P. Sutton, Electron-energy-loss spectra and the structural stability of nickel oxide: An LSDA+U study, Phys. Rev. B **57**, 1505 (1998).

[46] A. A. Mostofi, J. R. Yates, G. Pizzi, Y.-S. Lee, I. Souza, D. Vanderbilt, and N. Marzari, An updated version of wannier90: A tool for obtaining maximally-localised Wannier functions, Comput. Phys. Commun. **185**, 2309 (2014).

[47] Q. Wu, S. Zhang, H.-F. Song, M. Troyer, and A. A. Soluyanov, WannierTools: An open-source software package for novel topological materials, Comput. Phys. Commun. **224**, 405 (2018).

[48] J. Cano, B. Bradlyn, Z. Wang, L. Elcoro, M. G. Vergniory, C. Felser, M. I. Aroyo, and B. A. Bernevig, Topology of Disconnected Elementary Band Representations, Phys. Rev. Lett. **120**, 266401 (2018).

[49] L. Elcoro, B. Bradlyn, Z. Wang, M. G. Vergniory, J. Cano, C. Felser, B. A. Bernevig, D. Orobengoa, G. de la Flor, and M. I. Aroyo, Double cryst. groups and their representations on the bilbao crystallographic server, J. Appl. Cryst. **50**, 1457 (2017).

[50] M. G. Vergniory, L. Elcoro, C. Felser, N. Regnault, B. A. Bernevig, and Z. Wang, A complete catalogue of high-quality topological materials, Nature (London) **566**, 480 (2019).

[51] G. Dhakal, M. M. Hosen, A. Ghosh, C. Lane, K. Gornicka, M. J. Winiarski *et al.*, Observation of topological surface state in a superconducting material, arXiv:1911.08519.

[52] C. Lane, M. M. Piva, P. F. S. Rosa, and J.-X. Zhu, Competition between electronic correlations and hybridization in $CaMn_2Bi_2$, arXiv:1911.10122.

[53] M. U. Muzaffar, S. Zhang, P. Cui, J. He, and Z. Zhang, Antisite defect-enhanced thermoelectric performance of topological crystalline insulators, Adv. Funct. Mater. **30**, 2003162 (2020).

[54] P. Giannozzi, S. Baroni, N. Bonini, M. Calandra, R. Car, C. Cavazzoni *et al.*, Quantum espresso: a modular and open-source software project for quantum simulations of materials, J. Phys.: Condens. Matter. **21**, 395502 (2009).

[55] N. Troullier and J. L. Martins, Efficient pseudopotentials for plane-wave calculations, Phys. Rev. B **43**, 1993 (1991).

[56] W. L. McMillan, Transition temperature of strong-coupled superconductors, Phys. Rev. **167**, 331 (1968).

[57] P. B. Allen and R. C. Dynes, Transition temperature of strong-coupled superconductors reanalyzed, Phys. Rev. B **12**, 905 (1975).

[58] F. Giustino, Electron-phonon interactions from first principles, Rev. Mod. Phys. **89**, 015003 (2017).

[59] S. Nosé, A unified formulation of the constant temperature molecular dynamics methods, J. Chem. Phys. **81**, 511 (1984).

[60] W. Qin, L. Li, and Z. Zhang, Chiral topological superconductivity arising from the interplay of geometric phase and electron correlation, Nat. Phys. **15**, 796 (2019).

[61] A. Kjekshus and K. Walseth, On the Properties of the $Cr_{1+x}Sb$, $Fe_{1+x}Sb$, $Co_{1+x}Sb$, $Ni_{1+x}Sb$, $Pd_{1+x}Sb$, and $Pt_{1+x}Sb$ Phases, Acta. Chem. Scand. **23**, 2621 (1969).

[62] P. Amornpitoksuk, D. Ravot, A. Mauger, and J. C. Tedenac, Structural and magnetic properties of the ternary solid solution between CoSb and $Fe_{1+\delta}Sb$, Phys. Rev. B **77**, 144405 (2008).

[63] K. Wittel and R. Manne, Atomic spin-orbit interaction parameters from spectral data for 19 elements, Theoret. Chim. Acta **33**, 347 (1974).

[64] D.-Y. Liu, Z. Sun, F. Lu, W.-H. Wang, and L.-J. Zou, Correlation-driven Lifshitz transition in electron-doped iron selenides (Li,Fe)OHFeSe, Phys. Rev. B **98**, 195137 (2018).

[65] H. Kontani and S. Onari, Orbital-Fluctuation-Mediated Superconductivity in Iron Pnictides: Analysis of the Five-Orbital Hubbard-Holstein Model, Phys. Rev. Lett. **104**, 157001 (2010).

[66] F. Wang and D.-H. Lee, The electron-pairing mechanism of iron-based superconductors, Science **332**, 200 (2011).

[67] A. Chubukov, Pairing mechanism in Fe-based superconductors, Annu. Rev. Condens. Matter Phys. **3**, 57 (2012).

[68] A. V. Chubukov, M. Khodas, and R. M. Fernandes, Magnetism, Superconductivity, and Spontaneous Orbital Order in Iron-Based Superconductors: Which Comes First and Why? Phys. Rev. X **6**, 041045 (2016).

[69] S. Mandal, R. E. Cohen, and K. Haule, Strong pressure-dependent electron-phonon coupling in FeSe, Phys. Rev. B **89**, 220502(R) (2014).

[70] Z. P. Yin, A. Kutepov, and G. Kotliar, Correlation-Enhanced Electron-Phonon Coupling: Applications of GW and Screened Hybrid Functional to Bismuthates, Chloronitrides, and Other High-T_c Superconductors, Phys. Rev. X **3**, 021011 (2013).

[71] C. H. P. Wen, H. C. Xu, Q. Yao, R. Peng, X. H. Niu, Q. Y. Chen, Z. T. Liu, D. W. Shen, Q. Song, X. Lou, Y. F. Fang, X. S. Liu, Y. H. Song, Y. J. Jiao, T. F. Duan, H. H. Wen, P. Dudin, G. Kotliar, Z. P. Yin, and D. L. Feng, Unveiling the Superconducting Mechanism of $Ba_{0.51}K_{0.49}BiO_3$, Phys. Rev. Lett. **121**, 117002 (2018).

[72] Z. R. Ye, Y. Zhang, F. Chen, M. Xu, J. Jiang, X. H. Niu, C. H. P. Wen, L. Y. Xing, X. C. Wang, C. Q. Jin, B. P. Xie, and D. L. Feng, Extraordinary Doping Effects on Quasiparticle Scattering and Bandwidth in Iron-Based Superconductors, Phys. Rev. X **4**, 031041 (2014).

[73] B. Lei, Z. J. Xiang, X. F. Lu, N. Z. Wang, J. R. Chang, C. Shang, A. M. Zhang, Q. M. Zhang, X. G. Luo, T. Wu, Z. Sun, and X. H. Chen, Gate-tuned superconductor-insulator transition in (Li,Fe)OHFeSe, Phys. Rev. B **93**, 060501(R) (2016).

[74] S. He, J. He, W. Zhang, L. Zhao, D. Liu, X. Liu *et al.*, Phase diagram and electronic indication of high-temperature superconductivity at 65 K in single-layer FeSe films, Nat. Mater. **12**, 605 (2013).

[75] W. Zhang, Z. Li, F. Li, H. Zhang, J. Peng, C. Tang, Q. Wang, K. He, X. Chen, L. Wang, X. Ma, and Q.-K. Xue, Interface charge doping effects on superconductivity of single-unit-cell FeSe films on SrTiO$_3$ substrates, Phys. Rev. B **89**, 060506(R) (2014).

[76] J. Shiogai, Y. Ito, T. Mitsuhashi, T. Nojima, and A. Tsukazaki, Electric-field-induced superconductivity in electrochemically etched ultrathin FeSe films on SrTiO$_3$ and MgO, Nat. Phys. **12**, 42 (2015).

[77] B. Lei, J. H. Cui, Z. J. Xiang, C. Shang, N. Z. Wang, G. J. Ye, X. G. Luo, T. Wu, Z. Sun, and X. H. Chen, Evolution of High-Temperature Superconductivity from a Low-T_c Phase Tuned by Carrier Concentration in FeSe Thin Flakes, Phys. Rev. Lett. **116**, 077002 (2016).

[78] S. N. Rebec, T. Jia, C. Zhang, M. Hashimoto, D. H. Lu, R. G. Moore, and Z. X. Shen, Coexistence of Replica Bands and Superconductivity in FeSe Monolayer Films, Phys. Rev. Lett. **118**, 067002 (2017).

[79] Z. Song, T. Zhang, Z. Fang, and C. Fang, Quantitative mappings between symmetry and topology in solids, Nat. Commun. **9**, 3530 (2018).

[80] N.-N. Zhao, P.-J. Guo, X.-Q. Lu, Q. Han, K. Liu, and Z.-Y. Lu, Topological properties of Mo$_2$C and W$_2$C superconductors, Phys. Rev. B **101**, 195144 (2020).

[81] L. Fu and C. L. Kane, Superconducting Proximity Effect and Majorana Fermions at the Surface of a Topological Insulator, Phys. Rev. Lett. **100**, 096407 (2008).

[82] L. Fu, C. L. Kane, and E. J. Mele, Topological Insulators in Three Dimensions, Phys. Rev. Lett. **98**, 106803 (2007).

[83] L. Fu and C. L. Kane, Topological insulators with inversion symmetry, Phys. Rev. B **76**, 045302 (2007).

[84] S. Medvedev, T. M. McQueen, I. A. Troyan, T. Palasyuk, M. I. Eremets, R. J. Cava, S. Naghavi, F. Casper, V. Ksenofontov, G. Wortmann, and C. Felser, Electronic and magnetic phase diagram of β-Fe$_{1.01}$Se with superconductivity at 36.7 K under pressure, Nat. Mater. **8**, 630 (2009).

[85] M. X. Chen, W. Chen, Z. Zhang, and M. Weinert, Effects of magnetic dopants in (Li$_{0.8}$M$_{0.2}$OH)FeSe (M = Fe, Mn, Co): Density functional theory study using a band unfolding technique, Phys. Rev. B **96**, 245111 (2017).

[86] N. Hao and S.-Q. Shen, Topological superconducting states in monolayer FeSe/SrTiO$_3$, Phys. Rev. B **92**, 165104 (2015).